

Emergence of Unitarity and Locality from Hidden Zeros at One-Loop

Jeffrey V. Backus^{1*} and Laurentiu Rodina^{2†}

¹*Joseph Henry Laboratories, Princeton University, Princeton, NJ 08544, USA, and*

²*Beijing Institute of Mathematical Sciences and Applications (BIMSA), Beijing, 101408, China*

Recent investigations into the geometric structure of scattering amplitudes have revealed the surprising existence of “hidden zeros”: secret kinematic loci where tree-level amplitudes in $\text{Tr}(\phi^3)$ theory, the Non-Linear Sigma Model (NLSM), and Yang-Mills theory vanish. In this letter, we propose the extension of hidden zeros to one-loop-order in $\text{Tr}(\phi^3)$ theory and the NLSM using the “surface integrand” technology introduced by Arkani-Hamed et al. We demonstrate their power by proving that, under the assumption of locality, one-loop integrands in $\text{Tr}(\phi^3)$ are unitary if and only if they satisfy the loop hidden zeros. We also present strong evidence that the hidden zeros themselves contain the constraints from locality, leading us to conjecture that the one-loop $\text{Tr}(\phi^3)$ integrand can be fixed by hidden zeros from a generically non-local, non-unitary ansatz. Near the one-loop zeros, we uncover a simple factorization behavior and conjecture that NLSM integrands are fixed by this property, also assuming neither locality nor unitarity. This work represents the first extension of such uniqueness results to loop integrands, demonstrating that locality and unitarity emerge from other principles even beyond leading order in perturbation theory.

INTRODUCTION

Scattering amplitudes provide fascinating insights into the structure of quantum field theory (QFT). The bootstrap approach, which seeks to bypass traditional off-shell methods by determining amplitudes directly from imposing a set of basic physical principles, has emerged as a powerful framework in their study — uncovering unexpected simplicity, efficient computational techniques, and novel mathematical structures. Such remarkable findings are persistent across a broad range of theories, from scalar theories like $\text{Tr}(\phi^3)$ and the Non-Linear Sigma Model (NLSM) to Yang-Mills and gravity. (See Refs. [1, 2] for reviews.)

A natural objective within this bootstrap perspective is to identify the minimal set of constraints sufficient to uniquely determine scattering amplitudes. Recently, a series of uniqueness theorems has revealed that the physical principles used to constrain amplitudes often constitute an *overdetermined* system [3–9], implying that naively distinct physical principles are, in fact, *not* independent. Most surprisingly, unitarity — and in some cases locality — were shown to emerge for free from other principles, such as gauge invariance, infrared (IR) behavior, ultraviolet (UV) scaling, or the color-kinematics duality. That these two foundational axioms of QFT are somehow emergent is not an unfamiliar statement: from a holographic perspective, the unitary and local bulk evolution encoded in the S-matrix is expected to emerge from new properties at asymptotic infinity, phrased only in terms of on-shell momenta.

The latest addition to this suite of defining principles is the “hidden zeros” [10]—specific kinematic configurations of external particle degrees of freedom where amplitudes vanish. (See also Refs. [11–15].) This property, totally obscured in the Feynman formulation, is remarkably generic, cropping up in theories of colored scalars,

pions, gluons, and, via the double copy [16–18], galileons and gravitons [19, 20]. In earlier work [9], it was proved that tree-level amplitudes in $\text{Tr}(\phi^3)$ theory are uniquely determined by hidden zeros under the assumption of locality, with unitarity (in the sense of factorization) an automatic consequence. This work also provided the first sharp equivalence between distinct principles: hidden zeros were shown to be equivalent to a secret enhanced Britto-Cachazo-Feng-Witten (or UV) scaling under non-adjacent shifts.

One of the greatest challenges in this uniqueness program has been extending these results beyond tree-level. If locality and unitarity are indeed to be regarded as emergent properties, it is crucial that we demonstrate this beyond leading order. However, finding such a uniqueness theorem at loop integrand level was previously considered not only difficult but fundamentally ill-defined. The notion of a unique loop integrand is ambiguous for two reasons: (1) internal loop momenta tailored to individual Feynman diagrams can be changed arbitrarily without affecting the physical amplitude, and (2) in massless theories, one manually tosses out “1 / 0” terms arising from tadpole and external bubble contributions, artificially destroying any single-loop cut structure in the integrand.

It is well-known that one can ameliorate the first issue by working in the planar limit $N \rightarrow \infty$, where a global loop variable can be defined. Remarkably, a novel resolution to the second problem appeared alongside the study of hidden zeros. The development of “surface kinematics” [21–27] provides a canonical definition of loop integrands (“surface integrands”) endowed with tremendous structure, making it now possible to address the question of uniqueness beyond tree-level. Within surface kinematics, there is a natural means of accommodating contributions from tadpoles and external bubbles, in such a way that all single-loop cuts precisely match the expected tree

amplitudes with totally generic kinematics.

In this letter, taking as example $\text{Tr}(\phi^3)$ theory and the NLSM, we show that these surface integrands can indeed be uniquely fixed at one-loop-order, with both locality and unitarity emerging from purely on-shell constraints. To do this, we first describe the kinematic mesh that neatly organizes kinematic data relevant for one-loop surface integrands [28, 29]. We then propose the one-loop generalization of the hidden zeros discovered at tree-level in Ref. [10]. Quite nicely, these zeros are maximal triangles (“big mountains”) on the one-loop mesh, in analogy to maximal rectangles on the tree-level mesh. In fact, our approach demonstrates that the various shapes of tree-level zeros have a *unified* origin in different single-loop cuts of surface integrands.

Near the big mountains, we uncover a novel one-loop factorization pattern in $\text{Tr}(\phi^3)$ and the NLSM:

$$\mathcal{I}_n^{\text{one-loop}}(c_\star \neq 0) = \left(\frac{c_\star}{X_L X_R} \right) \times \mathcal{A}_{n+2}^{\text{tree}}, \quad (1)$$

where the kinematic dependence on the *r.h.s.* is dictated by a simple graphical rule on the one-loop mesh. Note that, unlike the traditional factorization patterns near singularities due to unitarity, this factorization and the analogous ones at tree-level (described in Refs. [10, 30, 31]) occur near *zeros* and fit naturally within the associahedron picture of scattering in $\text{Tr}(\phi^3)$ theory [32]. What’s more, as we will describe, this factorization pattern is even distinct from the integrand “split” configurations introduced in Ref. [24].

With these results in-hand, we prove that, under the assumption of locality, the $\text{Tr}(\phi^3)$ integrand is unitary *if and only if* it satisfies the big mountain zeros. Note that this is a *highly* non-trivial statement: the number of terms to fix in a non-unitary, local ansatz grows exponentially with multiplicity, while the number of zero constraints grows linearly! We then present strong evidence that, starting from a non-local, non-unitary ansatz, big mountain zeros are still sufficient to uniquely determine the $\text{Tr}(\phi^3)$ integrand. Finally, assuming neither locality nor unitarity, we conjecture that the strictly stronger requirement of factorization near zeros in Eq. (1) is sufficient to uniquely fix the NLSM integrand. Our results generalize similar findings at tree-level, implying for the first time non-trivial connections between physical principles across higher orders in perturbative QFT.

REVIEW: THE KINEMATIC MESH AND ZEROS AT TREE-LEVEL

We will begin by reviewing the story at tree-level. In scalar theories, the kinematic data for an n -point scattering amplitude is specified by the momenta of all external particles k_i^μ , satisfying momentum conservation and the

on-shell condition. The scattering amplitude is then a rational function of Lorentz-invariant products of these momenta $k_i \cdot k_j$. In theories with *colored* scalars (the subject of this paper), we can decompose the full amplitude into a sum over color-ordered amplitudes, each of which only receives contributions from planar diagrams. Any of these “partial amplitudes” can then be written solely in terms of the planar variables $X_{i,j} = (k_i + k_{i+1} + \dots + k_{j-1})^2$. Non-planar invariants $c_{i,j} = -2k_i \cdot k_j$ for i, j not adjacent are related to the planar variables by

$$c_{i,j} = X_{i,j} + X_{i+1,j+1} - X_{i,j+1} - X_{i+1,j}. \quad (2)$$

It is these color-ordered amplitudes (or, more precisely, the analogous color-ordered integrands) that we will bootstrap in the present work.

We can represent the necessary kinematic data for an n -point scattering process using the tree-level “momentum disk,” drawn on the *l.h.s.* of Fig. 1. On the boundary of the disk, we draw n marked points, and we label the segments between them by null external momenta. Each full triangulation corresponds to a Feynman diagram in $\text{Tr}(\phi^3)$ theory, with chords $X_{i,j}$ representing inverse propagators, and the amplitude is obtained by summing over all possible triangulations. Similarly, NLSM amplitudes correspond to even-angulations of the disk [23].

In this work, we’ll also find it useful to organize both planar and non-planar kinematic data with the tree-level “kinematic mesh”; see the *r.h.s.* of Fig. 1 for examples. Each vertex in the mesh belongs to an X , and each diamond is labeled by a $c_{i,j}$ whose indices match the $X_{i,j}$ at the bottom of its diamond. We can then read off the relation in Eq. (2) for any $c_{i,j}$ by summing the two X ’s at the top and bottom of its diamond and subtracting by the two X ’s on the left and right.

In Ref. [10], it was shown that color-ordered amplitudes in $\text{Tr}(\phi^3)$ and the NLSM vanish when all c ’s in any maximal rectangle on the mesh are set to zero (the “hidden zeros”). We can categorize any one of these zeros as a (k, m) -zero, corresponding to the set:

$$\begin{aligned} c_{i,j} &= 0, \quad i \in \{m, m+1, \dots, m+k-1\}, \\ j &\in \{k+m+1, k+m+2, \dots, m-2+n\}, \end{aligned} \quad (3)$$

where k is the “thickness” of the zero as drawn on the mesh and m is the index that appears in all c ’s in its bottom (rightward-moving) row. (See Fig. 1 for examples.) The hidden zero configurations are then precisely equivalent to these (k, m) -zeros for all $k = 1, 2, \dots, n-4$ and $m = 1, 2, \dots, n$. Surprisingly, the authors of Ref. [10] observed that, in examples at low multiplicity, the hidden zeros were sufficient to fix the $\text{Tr}(\phi^3)$ amplitude from a generically non-local, non-unitary ansatz.

Since they play a crucial role in the present work, let us review the constraints locality and unitarity impose on color-ordered scattering amplitudes. At tree-level, locality demands that all singularities of the amplitude occur

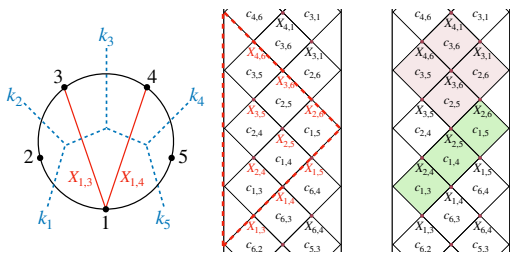


FIG. 1: Left: The momentum disk at five-points overlaid with a particular triangulation and its dual Feynman diagram in $\text{Tr}(\phi^3)$. Middle: The six-point kinematic mesh, with an outlined sub-region containing each planar invariant once (a “ray triangulation”). Right: The rectangles corresponding to the (1,1)-zero (in green) and the (2,2)-zero (in red).

as simple poles in planar invariants $X_{i,j}$, and that any two X 's only appear in a denominator together if they are compatible. By compatible, we mean that they are both propagators in a particular Feynman diagram; or, in surface language, that their corresponding chords on the momentum disk do not cross. Unitarity, through the optical theorem, dictates that the residue on any pole of a tree-level amplitude must factorize into a product of appropriate lower-point amplitudes. This pattern is most cleanly evinced from the momentum disk: cutting a chord $X_{i,j}$ breaks the disk into two sub-disks, which each give the multiplicity and kinematics of the lower-point amplitudes that appear due to unitarity.

Starting from a local (but non-unitary) ansatz for the n -point tree-level amplitude in $\text{Tr}(\phi^3)$ theory, Ref. [9] proved that imposing at most $n - 3$ distinct $(1, m)$ -zero conditions restricts us to the $\text{Tr}(\phi^3)$ amplitude, up to an overall normalization. Said more precisely, taking as ansatz an arbitrary linear combination of all n -point Feynman diagrams in $\text{Tr}(\phi^3)$ theory with different weights a_i , hidden zeros fix all $a_i = a$, guaranteeing unitarity is satisfied on every cut. As a result, we see that unitarity at tree-level is an *automatic* result of hidden zeros and locality.

THE KINEMATIC MESH AND ZEROS AT ONE-LOOP

Let us now see how this surface picture extends to loop-level. In scalar theories, while the loop-integrated amplitude is generically a complicated transcendental function, the loop *integrand* is a rational function of external and loop momenta, in many ways similar to the tree-level amplitude. In colored theories where we take the planar limit $N \rightarrow \infty$, dual variables provide a way to put all one-loop diagrams under a global loop integration and perform the same color decomposition we did at tree-

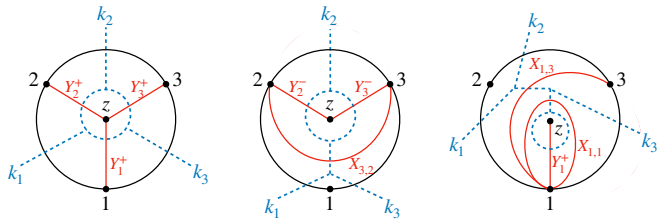


FIG. 2: The one-loop surface picture for kinematic variables and dual Feynman diagrams in $\text{Tr}(\phi^3)$ theory, including tadpoles (right), external bubbles (middle), and propagator doubling $Y \rightarrow Y^\pm$ (throughout).

level. In this case, there exists a canonical one-loop *surface* integrand in $\text{Tr}(\phi^3)$ and the NLSM endowed with both a momentum disk and a kinematic mesh, which we now describe.

At one-loop, the analog of the tree-level momentum disk is the *punctured* momentum disk, where we add a puncture z to the bulk of the tree disk, as shown in Fig. 2. The inclusion of the puncture introduces some new properties of chords on this surface not present at tree-level but critical to describing the surface integrand. For example, using the convention that $X_{i,j}$ denotes a chord that wraps around the puncture in increasing order from i to j (when $i, j \neq z$), it is clear from the surface picture that $X_{i,j} \neq X_{j,i}$, even though naively by momentum homology these two should be equal. What's more, the surface includes these curves that obviously *vanish* by homology, such as the chords $X_{i,i}$ that start on i , wrap around the puncture once, and return to i . (See the *r.h.s.* of Fig. 2 for an example.) On the other hand, the puncture introduces new variables $X_{i,z} = Y_i$ whose curves start on i and end on the puncture. These are the variables that, when using homology, depend on the internal loop momentum l^μ : fixing, *e.g.*, $Y_1 = l^2$, we have $Y_i = (l + p_1 + \dots + p_{i-1})^2$ for the rest. For reasons that will become clear in a moment, we will also need to equip the puncture with a parity $Y_i \rightarrow Y_i^\pm$, and then take the sum of the integrand with all loop variables positive Y_i^+ and the integrand with all loop variables negative Y_i^- [28, 29]. In what follows, when we refer to *the* loop integrand, we mean precisely this “doubled” version.

As a result of these observations, in order to define our one-loop surface integrand we must move past obtaining kinematic variables by homology and instead work with a new, larger kinematic space defined *purely* by curves on the punctured disk [25]. Doing so comes at the cost of introducing many more terms into our integrands than play a role post-loop-integration. For example, as shown in Fig. 2, each triangulation with a curve $X_{i,i}$ corresponds to a $\text{Tr}(\phi^3)$ diagram with a tadpole, and those with $X_{i+1,i}$ (and no $X_{i,i}$) have massless external bubbles—scaleless contributions to the integrand which famously vanish in dimensional regularization after integrating. To get back

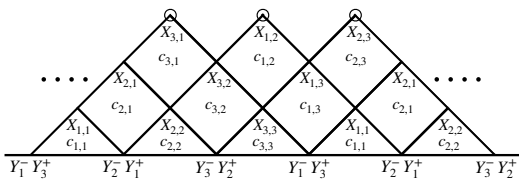


FIG. 3: The Y^-Y^+ kinematic mesh of the three-point, one-loop integrand.

to the familiar integrand in momentum space, we can always take away the parity of the puncture, throw out scaleless contributions by hand, set $X_{i,j} = X_{j,i}$, and express the $X_{i,j}$ and Y_i in terms of external momenta k_i^μ and the loop momentum l^μ via homology. However, keeping these terms around gives us a structurally-rich definition of the loop integrand purely in terms of triangulations on a surface, where importantly all single-loop cuts are well-defined.

As a near-immediate benefit of this formalism, one can naturally organize the surface kinematic data using a one-loop kinematic mesh, an example of which is shown in Fig. 3. Note that the propagator doubling $Y_i \rightarrow Y_i^\pm$ is obviously crucial to the construction of the mesh.

As at tree-level, each (half) diamond in the one-loop mesh corresponds to a non-planar invariant $c_{i,j}$ whose indices now match those of the planar variable $X_{i,j}$ at the *top* of the diamond. In this case, how the c 's are related to the X 's is slightly different due to the Y variables at the bottom of the mesh. For $c_{i,i}$ and $c_{i+1,i}$, we define

$$\begin{aligned} c_{i,i} &= X_{i,i} - Y_i^- - Y_i^+, \\ c_{i+1,i} &= X_{i+1,i} - X_{i,i} - X_{i+1,i+1} + Y_{i+1}^- + Y_i^+, \end{aligned} \quad (4)$$

while, for all others, we have

$$c_{i,j} = X_{i,j} + X_{i-1,j+1} - X_{i,j+1} - X_{i-1,j}. \quad (5)$$

The zeros on this mesh correspond to setting all c 's in a maximal triangle (a “big mountain”) to zero. That is, to impose the zero corresponding to the peak labeled by $c_{i-1,i} = 0$, we need to set

$$c_{m,k} = 0, \quad m \in \{k, k+1, \dots, i-1\}, \quad (6)$$

for each $k = 1, 2, \dots, n$. Since these zeros can only be phrased with surface kinematics, their existence is totally obscured in a generic integrand written in terms of momenta. In Appx. C, we will prove that imposing any of these big mountain zeros forces the integrands in both $\text{Tr}(\phi^3)$ theory and the NLSM to vanish.

Note that we can equally define a mesh with “ $-$ ” and “ $+$ ” switched in Fig. 3, leading to another set of hidden zeros. Hence, the n -point one-loop integrand has $2n$ big mountain zeros. We will denote the zero with peak at $c_{i-1,i} = 0$ and ordering $Y^\pm Y^\mp$ as the (i, \pm) -zero of the one-loop mesh. In Appx. C, we will show that these

zero configurations are actually *degenerate*; that is, the integrand satisfies all $(i, +)$ -zeros if and only if it satisfies all $(i, -)$ -zeros.

Finally, let us specify exactly what locality and unitarity mean in the context of this surface integrand. At tree-level, recall that we rephrased the requirements of these two principles in terms of the momentum disk: locality told us chords could not cross, and unitarity said that, on cuts through any set of chords, the amplitude needed to factorize in agreement with the disk. The natural generalization to loop-level is then the extension of these properties to the punctured disk. Note that, while these definitions guarantee that the physical loop-integrated amplitude is consistent with locality and unitarity, they constitute strictly stronger requirements, as they include rules for dealing with tadpoles and external bubbles that do not appear post-loop-integration.

Integrand Examples

Here we give a few examples of what the one-loop surface integrand looks like in $\text{Tr}(\phi^3)$ theory and the NLSM. In the simplest case of two points, the integrand for $\text{Tr}(\phi^3)$ is given by

$$\mathcal{I}_2^{\text{Tr}(\phi^3)} = \frac{1}{Y_1^+ Y_2^+} + \frac{1}{Y_1^+ X_{1,1}} + \frac{1}{Y_2^+ X_{2,2}} + (Y^+ \leftrightarrow Y^-). \quad (7)$$

One can easily verify by hand that the integrand vanishes on the four big mountains, the $(1, \pm)$ - and $(2, \pm)$ -zeros.

We also give here the three-point $\text{Tr}(\phi^3)$ integrand:

$$\begin{aligned} \mathcal{I}_3^{\text{Tr}(\phi^3)} &= \left[\frac{1}{Y_1^+ X_{1,1}} \left(\frac{1}{X_{2,1}} + \frac{1}{X_{1,3}} \right) + (\text{cyclic}) \right] + \\ &+ \left[\frac{1}{Y_2^+ Y_3^+ X_{3,2}} + (\text{cyclic}) \right] + \frac{1}{Y_1^+ Y_2^+ Y_3^+} + \\ &+ (Y^+ \leftrightarrow Y^-), \end{aligned} \quad (8)$$

which vanishes, for example, on the $(i, -)$ -zeros for $i = 1, 2, 3$ shown in Fig. 3.

As at tree-level, one may obtain an NLSM integrand through the δ -shift prescription [22]. To do this, we take the $\text{Tr}(\phi^3)$ integrand and shift its kinematics $X_{i,j}$ depending on whether i, j are even or odd: we take $X_{i,j} \rightarrow X_{i,j} + \delta_{i,j}$, where $\delta_{e,o} = \delta_{o,e} = 0$ and $\delta_{e,e} = \delta = -\delta_{o,o}$. We also shift Y_i^\pm in the same way, but we first have to choose whether to treat plus as even and minus as odd, or vice versa. After these shifts, we take the limit as $\delta \gg X, Y$ and pick out the leading term, which gives us two possibilities for the NLSM integrand. At two-points, these are

$$\mathcal{I}_{2,\pm}^{\text{NLSM}} = 2 - \frac{X_{2,2} + Y_1^\mp}{Y_2^\mp} - \frac{X_{1,1} + Y_2^\pm}{Y_1^\pm}, \quad (9)$$

where treating plus as even and minus as odd gives us the “ $+$ ” configuration. Regardless of this ambiguity, one

can verify that both expressions satisfy the same four big mountain zero conditions as Eq. (7). This is because both δ -shift conventions preserve the c 's given in Eqs. (4) and (5) for any multiplicity.

Factorization Near Zeros

In Ref. [10], it was shown that, when setting all $c_{i,j}$ to zero in a particular (k, m) -zero of the tree-level mesh except one $c_\star \neq 0$, the amplitude in either $\text{Tr}(\phi^3)$ or the NLSM factorizes into three pieces:

$$\mathcal{A}_n^{\text{tree}}(c_\star \neq 0) = \left(\frac{c_\star}{X_B X_T} \right) \times \mathcal{A}_{\text{down}}^{\text{tree}} \times \mathcal{A}_{\text{up}}^{\text{tree}}. \quad (10)$$

The first term is the same for any $c_\star \neq 0$ in a particular zero, whereas the kinematics and particle content of the two tree sub-amplitudes depend on c_\star , the zero, and whether we are describing $\text{Tr}(\phi^3)$ or the NLSM.

One can therefore imagine that a similar story holds for the one-loop integrand. Indeed, a factorization pattern is naturally suggested by looking at the mesh: if we delete any big mountain zero, what remains looks like a ‘‘ray triangulation’’ section from the $(n+2)$ -point tree-level mesh, with the two sides of the mountain forming its upper and lower boundaries. Since turning on any $c_\star \neq 0$ inside a (i, \mp) -zero sets $c_\star = Y_i^\mp + Y_{i-1}^\pm$, we might thus guess that the integrands in both $\text{Tr}(\phi^3)$ and the NLSM factorize as

$$\mathcal{I}_n(c_\star \neq 0) = \left(\frac{1}{Y_i^\mp} + \frac{1}{Y_{i-1}^\pm} \right) \times \mathcal{A}_{n+2}, \quad (11)$$

with tree-level amplitude \mathcal{A}_{n+2} depending on the kinematics in the remaining tree-level mesh with some modifications on its upper and lower boundaries.

For $\text{Tr}(\phi^3)$, this turns out to be exactly true. However, the situation is slightly more subtle for the NLSM. For example, let's say we chose to treat minus as odd and plus as even in the δ -shift prescription. The resulting NLSM integrand then factorizes as in Eq. (11) near $(i, -)$ -zeros when i is even and near $(i, +)$ -zeros when i is odd. To see factorization near the other zeros, we would need to consider the opposite-parity NLSM integrand where minus was treated as even and plus as odd.

In any case, whether we are considering $\text{Tr}(\phi^3)$ or the NLSM, the graphical rule for determining the kinematics of \mathcal{A}_{n+2} near a $(i, -)$ -zero is shown in Fig. 4. Of course, the rules for factorization near $(i, +)$ -zeros can be obtained by a simple parity transformation. We prove this factorization pattern in Appx. A.

Let's do a small example at three-points in $\text{Tr}(\phi^3)$ using Eq. (8). Working within the $(3, -)$ -zero, let's say we turn on $c_{1,3} \neq 0$. The implementation of the rules in Fig. 4 for this case are shown in Fig. 5: based on this, we

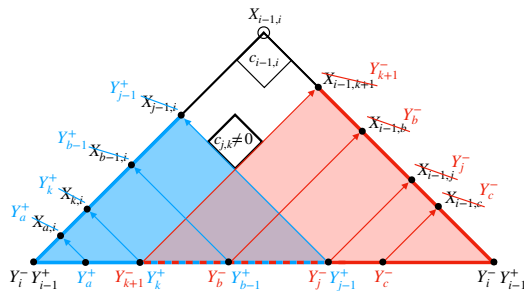


FIG. 4: Factorization of variables near a $(i, -)$ -zero with $c_{j,k} \neq 0$. The region below and beside $c_{j,k}$ is divided into blue and red parts. All the X variables on the slope of the mountain in a colored region are replaced with Y variables using the rule shown in the figure.

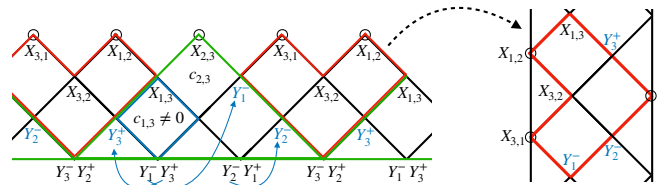


FIG. 5: Factorization of variables near the $(3, -)$ -zero at three-points. The green-outlined big mountain zero implicitly defines a red-outlined region, representing the mesh for a $(3+2)$ -point tree amplitude. Some of the X variables on this mesh are replaced by Y variables, according to the rules given in Fig. 4.

find that the factorization is

$$\mathcal{I}_3^{\text{Tr}(\phi^3)} \rightarrow \left(\frac{1}{Y_2^+} + \frac{1}{Y_3^-} \right) \times \mathcal{A}_5(X_{1,3}, Y_3^+, X_{3,2}, Y_1^-, Y_2^-), \quad (12)$$

where the five-point tree amplitude is given explicitly by

$$\mathcal{A}_5 = \frac{1}{Y_2^-} \left(\frac{1}{Y_1^-} + \frac{1}{X_{3,2}} \right) + \frac{1}{X_{1,3}} \left(\frac{1}{Y_3^+} + \frac{1}{Y_1^-} \right) + \frac{1}{X_{3,2} Y_3^+}. \quad (13)$$

In Ref. [24], special kinematic ‘‘split’’ configurations where the $\text{Tr}(\phi^3)$ integrand factorized into tree amplitudes were presented. However, the near-zero configurations we derive here are formally distinct from the ones covered by split kinematics, since our kinematic configurations always mix positive and negative parity propagator variables in nontrivial ways.

UNIQUENESS FROM ZEROS AT ONE-LOOP IN $\text{TR}(\phi^3)$

Assuming Locality

Having now understood the definition and structure of the surface integrand, let us prove that the one-loop

mesh zeros uniquely fix the color-ordered, *local* (but non-unitary) ansatz for the surface integrand \mathcal{M}_n in $\text{Tr}(\phi^3)$ theory. We will start with the same generically non-unitary ansatz as in Ref. [9]: an arbitrary linear combination of all full triangulations of the punctured disk. Using n of the big mountain zeros, we will prove that the weights are equal by showing that single-loop cuts are uniquely fixed. As we have referenced previously, taking a single-loop cut of the n -point surface integrand lands us precisely on an $(n+2)$ -point tree-level amplitude with generic kinematics. So, taking a single-loop cut of \mathcal{M}_n will give us a non-unitary ansatz for this $(n+2)$ -point tree-level amplitude \mathcal{B}_{n+2} . It then turns out that the combined big mountain zero and single-loop cut conditions for $n-1$ of the zeros *secretly* impose the known tree-level mesh zeros on \mathcal{B}_{n+2} , fixing it up to an overall normalization.

Let us see how this works in practice. We'll consider here the $(i, -)$ -zeros and the Y^+ cuts. (Different parity choices can be treated identically.) For simplicity, we'll focus on cutting Y_1^+ . The first thing we must do is prove that the operations of imposing a zero and taking a residue commute, since our assumption is the full integrand vanishes (not individual cuts). As long as $i \neq 2$, we find that

$$\text{Res}_{Y_1^+=0}(\mathcal{M}_n|_{(i,-)}) = \left(\text{Res}_{Y_1^+=0} \mathcal{M}_n \right)_{(i,-), Y_1^+=0}. \quad (14)$$

This is because, for $i \neq 2$, setting $Y_1^+ = 0$ on the support of an $(i, -)$ -zero does not force any other kinematic variables to vanish, ensuring the residues on both sides of Eq. (14) pick up the same terms. To contrast, for $i = 2$ the zero sets $Y_2^- = -Y_1^+$, so the residue on the *l.h.s.* will pick up extra terms as compared to the *r.h.s.* corresponding to the pole in Y_2^- .

Because it is our hypothesis that \mathcal{M}_n satisfies the big mountain zeros, we have the condition

$$\left(\text{Res}_{Y_1^+=0}(\mathcal{M}_n) \right)_{(i,-), Y_1^+=0} = \mathcal{B}_{n+2}(Z_{i,j})|_{(i,-), Y_1^+=0} = 0, \quad (15)$$

for all $i \neq 2$, where \mathcal{B}_{n+2} is our local tree-level ansatz with generic kinematics we denote by $Z_{i,j}$ to distinguish them from the loop $X_{i,j}$. It is simple to work out the mapping between the Z 's and the X/Y 's: the non-trivial ones are $Y_i^+ \leftrightarrow Z_{i,n+2} = Z_{n+2,i}$, $X_{i,1} \leftrightarrow Z_{i,n+1} = Z_{n+1,i}$, and $X_{1,i} \leftrightarrow Z_{i,1} = Z_{1,i}$ for $i = 2, 3, \dots, n$, and $X_{1,1} \leftrightarrow Z_{1,n+1}$. For the rest, we have $X_{i,j} \leftrightarrow Z_{i,j} = Z_{j,i}$ for $i < j$. (Note that $X_{i,j}$ with $i \geq j$ are always locally inconsistent with the Y_1^+ chord.) We show examples of how this works in Fig. 6.

Now, the local structure of \mathcal{B}_{n+2} in terms of Z variables defines a tree-level mesh which can easily be obtained graphically from the loop mesh, as we show in Fig. 7. It is then natural to ask what the $(i, -)$ -zero and $Y_1^+ = 0$ conditions induce at the level of the Z kinematics of the tree ansatz. Quite beautifully, for any $i \neq 2$, the

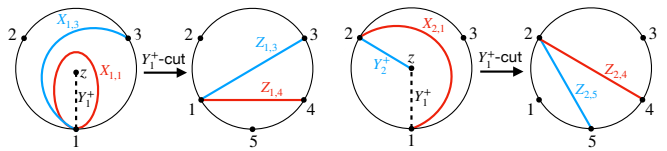


FIG. 6: The Y_1^+ cut of an n -point integrand induces a local triangulation of the $(n+2)$ -point tree-disk.

overlap of an $(i, -)$ -zero and the tree mesh of \mathcal{B}_{n+2} is exactly a maximal rectangle—a tree-level hidden zero! (See the blue diamonds in Fig. 8.) For diamonds that do not touch the right edge of the tree mesh, it is clear that the $c_{i,j}(X) = 0$ conditions of the loop zero trivially induce the corresponding $c_{i,j}(Z) = 0$ conditions in the tree mesh. For diamonds that do touch the right edge (but are not the bottom-most diamond), the mountain zero condition $c_{k,1}(X) = 0$ implies that

$$X_{k,1} + X_{k-1,2} = X_{k-1,1} + X_{k,2}. \quad (16)$$

But, we also have $X_{i,2} = Y_i^+ + Y_2^-$ for all $i \leq \max(k)$ on the support of the zero. So, Eq. (16) is equivalent to $X_{k,1} + Y_{k-1}^+ = X_{k-1,1} + Y_k^+$, which is exactly what appears on the overlap between the tree-mesh and loop-mesh in Fig. 8. Finally, for the bottom-most diamond, setting $c_{2,1} = 0$ and $Y_1^+ = 0$ tells us

$$X_{2,1} + Y_2^- = X_{1,1} + X_{2,2}. \quad (17)$$

Since we have $X_{2,2} = Y_2^+ + Y_2^-$ on the support of the zero, this condition matches what is shown in Fig. 8.

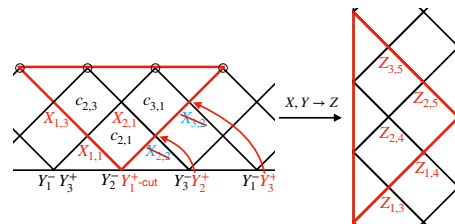


FIG. 7: The Y_1^+ cut defines the ray triangulation of an $(n+2)$ -point tree mesh, where the loop-level $X_{i,2}$ on the right edge are replaced with the corresponding Y_i^+ .

As a result of these arguments, the fact that \mathcal{B}_{n+2} vanishes on the zero+cut condition shown in Eq. (15) is *equivalent* to it vanishing on a tree-level hidden zero! In general, for a cut on Y_j^+ , an $(i, -)$ -loop-zero acts as a $(i-j-1, j)$ -tree-zero for all $i \neq j, j+1$, and as an $(1, n+1)$ -zero when $i = j$. (The mountain zero with $i = j+1$ has no overlap with the tree mesh, a paramount fact to-be-exploited later.) In Appx. B, we show that this set of zeros imposes identical constraints on \mathcal{B}_{n+2} as $(n+2) - 3$ distinct $(1, m)$ -zeros, which were revealed in Ref. [9] to be sufficient to fix \mathcal{B}_{n+2} to be the *unitary* amplitude \mathcal{A}_{n+2} up to an overall number. Obviously,

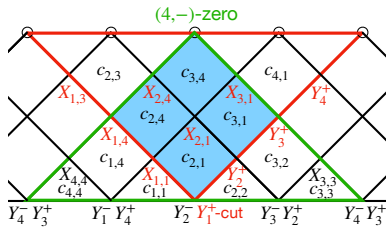


FIG. 8: The mountain zeros (green) intersect the mesh area corresponding to a tree amplitude (red) in maximal rectangular regions, producing the tree-level zeros.

there is overlap between all cuts involving the same parity Y^+ due to the term proportional to $1/Y_1^+ \cdots Y_n^+$ in \mathcal{M}_n . This implies all terms of positive parity have equal weight a^+ .

In the opposite parity case, the arguments above go through identically: the only difference is that the tree mesh shown in Fig. 7 now has the X 's on its *left* edge replaced with the corresponding Y^- variables. So, since each term in \mathcal{M}_n has at least one Y , we find that the ansatz must take the form

$$\mathcal{M}_n = a^+ \mathcal{I}_n^+ + a^- \mathcal{I}_n^-, \quad (18)$$

where \mathcal{I}_n^\pm is the part of the n -point one-loop integrand with only Y^\pm poles.

The final step is then proving $a^+ = a^-$. To do this, let us impose the $(2,-)$ -zero and cut Y_1^+ . Note that this is exactly the choice where the tree mesh has no overlap with the mountain zero. On this zero, we have $Y_1^+ = -Y_2^-$, and so we get

$$\left(a^+ \mathcal{A}_{n+2}^{(1)} - a^- \mathcal{A}_{n+2}^{(2)} \right)_{(2,-), Y_1^+=0} = 0, \quad (19)$$

where $\mathcal{A}_{n+2}^{(1)}$ is the tree amplitude resulting from the cut in Y_1^+ and $\mathcal{A}_{n+2}^{(2)}$ is that for the cut in Y_2^- . Since these Y variables lie at the same point on the loop mesh, the interior of their tree meshes are identical (see Fig. 7); it is only on the edges that they may differ.

However, on the support of the zero+cut conditions, it is straightforward to show that the edges also exhibit identical kinematic dependence. As a result, we find that $\mathcal{A}_{n+2}^{(1)}$ and $\mathcal{A}_{n+2}^{(2)}$ are the *same* amplitude on the support of the zero+cut, and thus $a^+ = a^-$ for Eq. (19) to hold. This proves that n mountain zeros uniquely fix the local ansatz for one-loop integrands in $\text{Tr}(\phi^3)$ theory, and that, therefore, unitarity follows as an automatic consequence of our assumptions. Like in the tree-level case, the number of weights in our one-loop ansatz grows exponentially with n , making the emergence of unitarity from hidden zeros and locality remarkably non-trivial.

Note that we needed to use only *half* of the $2n$ big mountain zeros (all with the same parity) to obtain this

result. (The arguments given above are structurally identical for the opposite parity $(i,+)$ -zeros.) In Appx. C, we show that this statement is really an equivalence: the local integrand ansatz \mathcal{M}_n is unitary *if and only if* it satisfies one parity-half of the $2n$ big mountain zeros!

Without Assuming Locality

We now drop the assumption of locality, and instead start with an ansatz consisting of any linear combination of terms with n poles, each of which can be any factor of $X_{i,j}$ or Y_i^\pm . The only technical requirement we make is that no term can contain both Y^- and Y^+ factors. Note that such an ansatz now grows *factorially* with multiplicity.

We have explicitly verified that the big mountain zeros are sufficient to fully constrain one-loop integrands up to four points, where the non-local, non-unitary ansatz contains around 6,500 terms, thus providing a highly non-trivial check. As a result, we make the stronger conjecture that both locality and unitarity emerge from hidden zeros at loop-level.

UNIQUENESS FROM FACTORIZATION NEAR ZEROS IN THE NLSM

Let us now examine the same questions of uniqueness from hidden zeros in the context of the NLSM one-loop integrand. In this case, a non-local, non-unitary $2n$ -point NLSM ansatz contains all terms with any n planar variables in the numerator and any n planar variables in the denominator, with the only restriction again being that opposite parity Y 's cannot appear together in the same term. Like in the $\text{Tr}(\phi^3)$ case, such an ansatz grows factorially with multiplicity.

Starting at four points, the zero conditions alone are insufficient to fully constrain the integrands, as it becomes possible to generate numerators that trivially satisfy all zeros [33]. However, this apparent inadequacy of the big mountain zeros also presents an opportunity to test the role of factorization near zeros — or, in bootstrap terms, to determine how much “amplitude information” this property encodes. Surprisingly, checking at four points explicitly, we find that this condition is sufficient to fully fix the non-local, non-unitary ansatz. Concretely, for all (i, \mp) -zeros (where plus corresponds to i odd and minus to i even), we require the ansatz satisfies a factorization of the type

$$\mathcal{M}_n(c_* \neq 0) \rightarrow \left(\frac{1}{Y_i^\mp} + \frac{1}{Y_{i-1}^\pm} \right) \times \mathcal{B}_{n+2}^{i,c_*}(\tilde{X}), \quad (20)$$

for all $c_* \neq 0$ within those zeros. Here, $B_{n+2}^{i,c_*}(\tilde{X})$ are non-local, non-unitary ansätze for the $(n+2)$ -point tree NLSM amplitude, different for each factorization, and the set \tilde{X} is the X, Y variables consistent with the graphical rule in Fig. 4. By construction, these constraints land us exactly on the four-point NLSM integrand where the plus in Y^+ was treated as even and minus in Y^- as odd in the δ -shift. In fact, these constraints uniquely fix both the *l.h.s.* and all *r.h.s.* amplitudes; the only required input is that of the universal prefactor, together with the allowed kinematic dependence of the *r.h.s.*! This is similar to how soft operators are sufficient to fully fix tree amplitudes which obey soft theorems [7].

For four points, the one-loop ansatz contains $\sim 25,000$ terms, making this observation very suggestive. We conjecture that factorization near zeros continues to fully determine NLSM integrands at arbitrary multiplicity, and that therefore both locality and unitarity are contained within this property!

OUTLOOK

In this letter, we demonstrated that one-loop integrands in two scalar theories can be uniquely determined by imposing novel constraints—loop hidden zeros and factorization near these zeros. Since our approach assumes neither locality nor unitarity, we have shown that these two seemingly fundamental principles of QFT can, in fact, be viewed as emergent, even beyond leading order in perturbation theory.

Strictly speaking, we have only proved this claim for a non-unitary, local $\text{Tr}(\phi^3)$ ansatz, where our argument revealed the surprising unification of all tree-level zeros in single-loop cuts of the surface integrand. A natural next step is thus to prove that hidden zeros are sufficient to fix the generically non-local, non-unitary $\text{Tr}(\phi^3)$ ansatz. Doing so promises to reveal other secret structures in the $\text{Tr}(\phi^3)$ surface integrand, but would likely first require a proof of the same fact at tree-level. Furthermore, it would be interesting to prove our conjecture that factorization near zeros is sufficient to uniquely fix the NLSM surface integrands.

Additionally, the surface kinematics framework applies at any loop order, and it can also be used to write down a Yang-Mills integrand with well-defined factorization on single-loop cuts [25]. Thus, a broad range of tests involving uniqueness and emergence from hidden zeros and factorization is now a tangible next step—beyond scalar theories, and at all orders in perturbation theory.

Acknowledgments—It is our pleasure to thank Carolina Figueiredo and Giulio Salvatori for insightful discussions and Nima Arkani-Hamed for helpful comments on the draft. JB is supported by the NSF Graduate Research

Fellowship under Grant No. KB0013612. LR is supported by the Beijing Natural Science Foundation International Scientist Project No. IS24014, and the National Natural Science Foundation of China General Program No. 12475070.

APPENDIX A: FACTORIZATION PROOF

Here, we prove the factorization formula (11). To do this, let us fix a particular $(i, -)$ -zero and $c_{a,b} \neq 0$ (the “loop near-zero” condition) and impose them on the $\text{Tr}(\phi^3)$ integrand \mathcal{I}_n . We can then cut on *any* Y_j^\pm , which will produce a particular tree amplitude \mathcal{A}'_{n+2} with generic kinematics on the support of the loop near-zero. For the moment, let us restrict so that we do not cut on Y_i^- or Y_{i-1}^+ . In this case, after imposing the loop near-zero condition, there are two options for \mathcal{A}'_{n+2} . If the overlap between the loop and tree meshes (as shown in Fig. 8) contains only c variables that vanish, then $\mathcal{A}'_{n+2} = 0$. If, alternatively, the overlap contains $c_{a,b} \neq 0$, the tree amplitude will factorize as given in Eq. (10). Looking at Fig. 8, we can easily pick out the universal prefactor for the factorization of \mathcal{A}'_{n+2} in this loop near-zero configuration: it is the four-point tree amplitude with kinematics given by the left-most and right-most corners of the overlap region. When cutting on a Y_j^+ , the right-most planar variable is always Y_{i-1}^+ . The left-most is $X_{j,i} = Y_i^- + Y_j^+ = Y_i^-$ on the cut. (The same story, with sides reversed, holds for cuts on Y_j^- .) So, we have

$$\mathcal{A}'_{n+2} \rightarrow \left(\frac{1}{Y_i^-} + \frac{1}{Y_{i-1}^+} \right) \times \mathcal{R}, \quad (21)$$

where \mathcal{R} is some function of planar variables we do not concern ourselves with now. This implies that all terms in \mathcal{I}_n with at least one Y that is neither Y_i^- nor Y_{i-1}^+ is proportional to the prefactor shown in Eq. (11).

When we cut on Y_i^- , we are left with a tree amplitude $\mathcal{A}_{n+2}^{(1)}$ whose mesh has no overlap with the zero. As such, it will neither vanish nor factorize. As discussed in Sec. 4.1, the kinematics of $\mathcal{A}_{n+2}^{(1)}$ are precisely those in the tree mesh formed as in Fig. 7 but instead with a shift on its left edge $X_{i-1,m} \rightarrow Y_m^-$ for all m . However, on the near loop-zero and cut, we also have $X_{m,i} = Y_m^+$ for all $m \leq a-1$ and $Y_i^- = X_{i,m}$ when $m > b+1$. Note that this derives, respectively, the rules in the blue and red triangles in Fig. 4. We can proceed with the same arguments for the cut on Y_{i-1}^+ , obtaining $\mathcal{A}_{n+2}^{(2)}$ whose tree mesh has the same interior as that of $\mathcal{A}_{n+2}^{(1)}$ and also undergoes the shifts drawn in Fig. 4 on the edges. So, $\mathcal{A}_{n+2} = \mathcal{A}_{n+2}^{(1)} = \mathcal{A}_{n+2}^{(2)}$ on this kinematic configuration.

Thus, we have shown that, on a near loop-zero, the integrand is proportional to the prefactor given Eq. (11),

and that this prefactor multiplies the tree amplitude \mathcal{A}_{n+2} with kinematics as shown in Fig. 4. So, we have proved Eq. (11) in $\text{Tr}(\phi^3)$ theory. As always, the proof for $(i, +)$ -zeros goes through in an identical manner.

Since the NLSM δ -shift leaves the nonplanar c variables unchanged, it commutes with imposing this near loop-zero kinematic configuration. So, the NLSM factorization can be derived from first going on the $\text{Tr}(\phi^3)$ factorization shown in Eq. (11) and then imposing the δ -shift prescription. However, in order to have the same factorization as $\text{Tr}(\phi^3)$, we must ensure that the Y variables in the universal prefactor do not get shifted. The factorization rules satisfying this requirement are given in the main text. Of course, the δ -shift will take us from $\mathcal{A}_{n+2}^{\text{Tr}(\phi^3)} \rightarrow \mathcal{A}_{n+2}^{\text{NLSM}}$ with the same kinematics shown in Fig. 4.

In Ref. [10], the analogous tree-level factorization was proved using classic “stringy” integrals that UV-complete $\text{Tr}(\phi^3)$ and NLSM tree-level amplitudes. In this work, we instead prove this factorization solely from from properties of the “low-energy” field-theory object \mathcal{I}_n .

APPENDIX B: TREE-LEVEL UNIQUENESS FROM DIVERSE ZEROS

In this Appendix, we show that a local function satisfying a series of $(1, m)$ -, $(2, m)$ -, $(3, m)$ -, \dots , (k, m) -zeros automatically satisfies the $(1, m)$ -, $(1, m + 1)$ -, \dots , $(1, m + k - 1)$ -zeros. For $k = n - 3$, this would imply a $\text{Tr}(\phi^3)$ local ansatz is uniquely fixed by either set of conditions.

To establish this, we use a result from Ref. [9], which states that a local function satisfies a (k, m) -zero if and only if it can be expressed as a sum over D -subsets, where each D -subset independently satisfies the (k, m) -zero condition. A D -subset consists of all n -point diagrams that can be obtained by attaching legs $(m, m + 1, \dots, m + k - 1)$ to an $(n - k)$ -point diagram. This is shown in Fig. 9 for a $(1, 2)$ -zero. Moreover, all diagrams within a D -subset must have equal weight. Therefore, to show that a function satisfies a particular $(1, m)$ -zero, we must show that all diagrams of the relevant D -subsets have equal weight.

We will demonstrate this for the simplest case, where the $(1, 1)$ - and $(2, 1)$ -zeros together imply the $(1, 2)$ -zero. The proof can easily be generalized to higher cases via induction.

Consider, to start, the diagrams in Fig. 10, which belong to the same D -subset for leg 2 and have legs 1 and 2 separated. If this subset satisfies the $(2, 1)$ -zero, it means all diagrams that can be obtained by removing legs 1 and 2 and attaching them anywhere else (respecting ordering and the relative structure of legs 1 and 2) must have equal weight. We are therefore free to keep leg 1 in its original position and simply place leg 2 in any desired

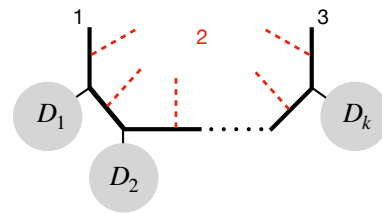


FIG. 9: A D -subset for leg 2 is formed by adding leg 2 in all possible ways to the lower point diagram defined by the sub-diagrams D_i . The subset satisfies a $(1, 2)$ -zero condition if and only if all such diagrams have equal weight.

location. This demonstrates that the $(2, 1)$ -zero enforces equal weights for all diagrams where legs 1 and 2 remain separated.

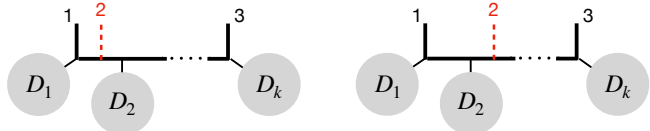


FIG. 10: Two diagrams of a particular D -subset for leg 2. We can obtain the *r.h.s.* diagram from the *l.h.s.* by removing legs 1 and 2, reattaching leg 1 to its original position, and translating leg 2. The existence of this $(2, 1)$ -zero mutation implies the two diagrams have equal weight.

The complete D -subset, however, includes the case where legs 1 and 2 form a two-particle pole, as illustrated on the *l.h.s.* of Fig. 11. Our goal is then to also relate this configuration to the previous diagrams. Since, for this diagram, the $(2, 1)$ -zero condition only permits the removal and reattachment of the full two-particle pole, we instead now use the $(1, 1)$ -zero to move leg 1 and separate it from leg 2. This transformation yields the diagram on the *r.h.s.* in Fig. 11, which now falls under the case just described. So, we’ve related diagrams with two-particle poles to those with legs 1 and 2 separate.

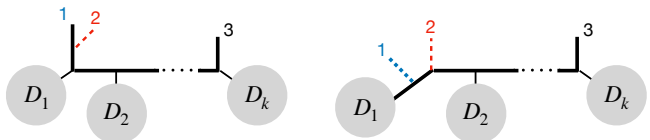


FIG. 11: These diagrams are also part of the same D -subset in Fig. 10, but are not directly related by a $(2, 1)$ -zero mutation. They are, however, related by a $(1, 1)$ -zero mutation.

This implies all diagrams of the D -subset for leg 2 in Fig. 9 have equal weight and therefore satisfy the $(1, 2)$ -

zero. The same argument can be applied for all different D -subsets, proving that any local function that satisfies a $(1, 1)$ - and a $(2, 1)$ -zero automatically satisfies the $(1, 2)$ -zero. This argument can be generalized by induction, proving our claim.

APPENDIX C: UNITARITY \Rightarrow BIG MOUNTAIN ZEROS

To finish the equivalence from the proof in Sec. 4.1, we need to demonstrate the following statement: if a particular $\mathcal{M}_n = \mathcal{M}_n^*$ does not satisfy some $(i_*, -)$ -zero, then some $a_i \neq a_j$.

We start by imposing the $(i_*, -)$ -zero on \mathcal{M}_n^* . Since each term in a local ansatz contains at least one Y variable as a pole, there are two possibilities. If, after imposing the zero, at least one term containing a pole in Y_i^- for $i \neq i_*$ or Y_j^+ for $j \neq i_* - 1$ in \mathcal{M}_n^* survives, we can freely cut on that variable, giving us the appropriate tree ansatz $\mathcal{B}_{n+2} \neq 0$ on the zero+cut condition. But, as shown in the main proof, the zero+cut condition on \mathcal{B}_{n+2} is equivalent to a tree-level zero. If all the weights in \mathcal{B}_{n+2} were equal, it would necessarily vanish on the this tree-level hidden zero, as demonstrated in Ref. [10]. Therefore, the fact that it doesn't means that some of the weights in \mathcal{M}_n^* must be unequal.

In the other case, the only Y variable that survives in \mathcal{M}_n^* on the support of the zero is $Y_{i_*}^- = -Y_{i_*-1}^+$. Then, cutting $Y_{i_*}^- = -Y_{i_*-1}^+$ tells us that the *difference* of two tree ansätze $\mathcal{B}_{n+2}^{(1)} - \mathcal{B}_{n+2}^{(2)} \neq 0$ on the support of the zero+cut, where $\mathcal{B}_{n+2}^{(1)}$ is what we get from cutting \mathcal{M}_n^* on $Y_{i_*}^-$ and $\mathcal{B}_{n+2}^{(2)}$ from cutting on $Y_{i_*-1}^+$, both away from the zero. As was demonstrated in the main proof, $\mathcal{B}_{n+2}^{(1)}$ and $\mathcal{B}_{n+2}^{(2)}$ on the support of the zero+cut are the *same* functions of planar variables, just with arbitrarily distinct coefficients a_i and b_i . The fact that the difference does not vanish therefore implies that $a_j \neq b_j$ for at least one j , and so the weights in \mathcal{M}_{n+1}^* are not all equal. Thus, we have completed the equivalence and shown that a $\text{Tr}(\phi^3)$ surface integrand is unitary *if and only if* it satisfies one parity-half of the $2n$ big mountain zeros!

Note that we could have just as well achieved the this result from using the $(i, +)$ -zeros. One immediate corollary is then that the local ansatz \mathcal{M}_n satisfies the positive-parity zeros if and only if it satisfies the negative-parity zeros. In this sense, either parity of zeros contains all information on big mountain zeros of the integrand. Another corollary is that the actual unitary one-loop surface integrand \mathcal{I}_n with $a_i = 1$ satisfies the $2n$ big mountain zeros. This is also true for the NLSM surface integrand, which is obtained from $\text{Tr}(\phi^3)$ from a c -preserving δ -shift. Like in the factorization proof given in Appx. A, we are able to prove the existence of these mountain zeros working entirely in field theory, without using stringy

integral techniques.

-
- * jvabackus@princeton.edu
† laurentiu.rodina@gmail.com
- [1] Z. Bern and J. Trnka, (2022), arXiv:2210.03146 [hep-th].
 - [2] G. Travaglini *et al.*, J. Phys. A **55**, 443001 (2022), arXiv:2203.13011 [hep-th].
 - [3] N. Arkani-Hamed, L. Rodina, and J. Trnka, Phys. Rev. Lett. **120**, 231602 (2018), arXiv:1612.02797 [hep-th].
 - [4] J. J. M. Carrasco and L. Rodina, Phys. Rev. D **100**, 125007 (2019), arXiv:1908.08033 [hep-th].
 - [5] L. Rodina, JHEP **09**, 078 (2019), arXiv:1612.03885 [hep-th].
 - [6] L. Rodina, JHEP **09**, 084 (2019), arXiv:1612.06342 [hep-th].
 - [7] L. Rodina, Phys. Rev. Lett. **122**, 071601 (2019), arXiv:1807.09738 [hep-th].
 - [8] L. Rodina, Phys. Rev. D **102**, 045012 (2020), arXiv:2005.06446 [hep-th].
 - [9] L. Rodina, Phys. Rev. Lett. **134**, 031601 (2025), arXiv:2406.04234 [hep-th].
 - [10] N. Arkani-Hamed, Q. Cao, J. Dong, C. Figueiredo, and S. He, (2023), arXiv:2312.16282 [hep-th].
 - [11] A. D'Adda, S. Sciuto, R. D'Auria, and F. Gliozzi, Nuovo Cim. 5A: No. 3, 421-32(1 Oct 1971). (1971), 10.1007/BF02723465.
 - [12] K. Zhou, (2024), arXiv:2411.07944 [hep-th].
 - [13] Y. Li, T. Wang, T. Brauner, and D. Roest, (2024), arXiv:2412.14858 [hep-th].
 - [14] Y. Zhang, (2024), arXiv:2412.15198 [hep-th].
 - [15] H. Huang, Y. Yang, and K. Zhou, (2025), arXiv:2502.07173 [hep-th].
 - [16] H. Kawai, D. C. Lewellen, and S. H. H. Tye, Nucl. Phys. B **269**, 1 (1986).
 - [17] Z. Bern, J. J. M. Carrasco, and H. Johansson, Phys. Rev. D **78**, 085011 (2008), arXiv:0805.3993 [hep-ph].
 - [18] Z. Bern, J. J. M. Carrasco, and H. Johansson, Phys. Rev. Lett. **105**, 061602 (2010), arXiv:1004.0476 [hep-th].
 - [19] C. Bartsch, T. V. Brown, K. Kampf, U. Oktem, S. Paranjape, and J. Trnka, (2024), arXiv:2403.10594 [hep-th].
 - [20] Y. Li, D. Roest, and T. ter Veldhuis, (2024), arXiv:2403.12939 [hep-th].
 - [21] N. Arkani-Hamed, H. Frost, G. Salvatori, P.-G. Plamondon, and H. Thomas, (2023), arXiv:2309.15913 [hep-th].
 - [22] N. Arkani-Hamed, Q. Cao, J. Dong, C. Figueiredo, and S. He, Phys. Rev. D **110**, 065018 (2024), arXiv:2401.05483 [hep-th].
 - [23] N. Arkani-Hamed and C. Figueiredo, (2024), arXiv:2403.04826 [hep-th].
 - [24] N. Arkani-Hamed and C. Figueiredo, (2024), arXiv:2405.09608 [hep-th].
 - [25] N. Arkani-Hamed, Q. Cao, J. Dong, C. Figueiredo, and S. He, (2024), arXiv:2408.11891 [hep-th].
 - [26] N. Arkani-Hamed, H. Frost, and G. Salvatori, (2024), arXiv:2412.21027 [hep-th].
 - [27] S. De, A. Pokraka, M. Skowronek, M. Spradlin, and A. Volovich, (2024), arXiv:2406.04411 [hep-th].
 - [28] N. Arkani-Hamed, S. He, G. Salvatori, and H. Thomas, JHEP **11**, 049 (2022), arXiv:1912.12948 [hep-th].
 - [29] N. Arkani-Hamed, H. Frost, G. Salvatori, P.-G. Plamondon,

- don, and H. Thomas, (to appear).
- [30] F. Cachazo, N. Early, and B. Giménez Umbert, *JHEP* **08**, 252 (2022), arXiv:2112.14191 [hep-th].
- [31] Q. Cao, J. Dong, S. He, C. Shi, and F. Zhu, *JHEP* **09**, 049 (2024), [Erratum: *JHEP* 01, 126 (2025)], arXiv:2406.03838 [hep-th].
- [32] N. Arkani-Hamed, Y. Bai, S. He, and G. Yan, *JHEP* **05**, 096 (2018), arXiv:1711.09102 [hep-th].
- [33] For the purposes of constructing amplitudes, one practical solution to obtain a unique result is to allow only same-parity terms in the numerator, *i.e.*, only $X_{e,e}$, $X_{o,o}$, and Y_e^+ and Y_o^- (when, for example, assigning $Y^{+/-}$ to be even/odd parity). This eliminates the trivial solutions and gives an efficient bootstrap procedure.